RSC Advances

PAPER

Check for updates

Cite this: *RSC Adv.*, 2018, **8**, 5127

Performance enhancement of a polydimethylsiloxane membrane for effective *n*-butanol pervaporation by bonding multi-silyl-functional MCM-41

Zhihao Si,†[a] Song Hu,†[a] Di Cai,[a] Peiyong Qin *[a] and Qinghong Xu *[b]

Received 7th October 2017
Accepted 22nd January 2018

DOI: 10.1039/c7ra11043j

rsc.li/rsc-advances

In the current work, MCM-41/polydimethylsiloxane (PDMS) mixed matrix membrane (MMM) was prepared for effective *n*-butanol pervaporation from a model aqueous solution. In order to improve the compatibility between MCM-41 and PDMS, different types of silane coupling agents including *n*-propyltrimethoxysilane (PTMS), *n*-octyltrimethoxysilane (OTMS), *n*-dodecyltrimethoxysilane (DTMS) and *n*-hexadecyltrimethoxysilane (HDTMS) were used to modify the MCM-41. The results showed that the highest *n*-butanol separation performance was achieved by bonding 20 wt% of PTMS-modified MCM-41 with PDMS. Under these conditions, total flux of 1476 g m^{-2} h^{-1} was obtained when separating a 1.5 wt% *n*-butanol aqueous solution at 55 °C. The total flux increased by nearly 40% compared to the pure PDMS membrane with no obvious changes of the *n*-butanol separation factor at the same time. The curing process of the casting solution was also significantly improved after MCM-41 modification.

Introduction

Pervaporation is a membrane based technology for sustainable and effective organics separation from diluted aqueous mixtures.[1] In recent years, in facing the problems of low productivity and low concentration in the *n*-butanol fermentation process, the separation of biobutanol from fermentation broths by pervaporation has been of great interest.[2–4] Compared with other separation techniques, pervaporation shows a relatively high selectivity, low energy requirement and is non-toxic.[1,5–7]

Most of the commercial pervaporation membranes for *n*-butanol separation are often prepared from organic polymers. However, the organic membranes were always limited by the trade-off between the organics permeability and the selectivity.[8] In comparison to this, the inorganic membranes not only exhibited higher thermal and chemical stabilities than the polymeric membranes, but also provided a rigid and robust structure with high swelling resistance.[9,10] Nevertheless, the high manufacturing cost of the inorganic membranes limited their industrial application.[4]

In order to overcome the above drawbacks of the organic and inorganic pervaporation membranes, mixed matrix membranes (MMMs) that filled with porous materials such as silicalite, zeolite, metal organic frameworks, silica and carbonaceous particles were widely applied for *n*-butanol separation,[11–18] which combined the superiorities of the two types of membranes.[19,20] In most of the cases, the improvement of the organics separation factors was more significant than the enhancement of the membrane flux after mixing the inorganic materials into the polymeric layers.

Lots of efforts have been made in preparing porous materials to improve membrane performance, especially membrane flux. It is because the membrane flux always negatively correlated with the pervaporation membranes cost.[21] In contrast to other inorganic additives, MCM-41, the mesoporous material, showed high specific surface (up to 1500 m^2 g^{-1}) and very narrow pore size distribution (2–10 nm).[22] The structure of MCM-41 is ordered one-dimensional linear channels like "honeycomb" (Fig. 1) and its larger pore structure would greatly improve the membrane flux when it was applied in pervaporation membrane preparation. In previous works, MCM-41 spheres were directly incorporated into a PDMS matrix for dimethylcarbonate/methanol azeotropic mixture separation. An optimized flux of 5256 g m^{-2} h^{-1} and a separation factor of 1.87 were obtained.[23] Jomekian *et al.* applied a polyethylene oxide (PEO)-MCM-41/polyvinylidene chloride (PVDC) nanocomposite membrane for the separation of bovine serum albumin.[24] The 20 wt% MCM-41-filled sodium alginate (NaAlg) nanocomposite membrane was also applied to separate the water/isopropanol (10 wt%) binary mixtures, providing a total flux and selectivity of 0.110 kg m^{-2} h^{-1} and 29 991, respectively.[25] However, in all of

[a]*Beijing Key Laboratory of Bioprocess, Beijing University of Chemical Technology, Beijing 100029, China. E-mail: qinpeiyong@tsinghua.org.cn*

[b]*State Key Laboratory of Chemical Resource Engineering, Beijing University of Chemical Technology, Beijing 100029, China. E-mail: xuqh@mail.buct.edu.cn*

† These authors contributed equally.

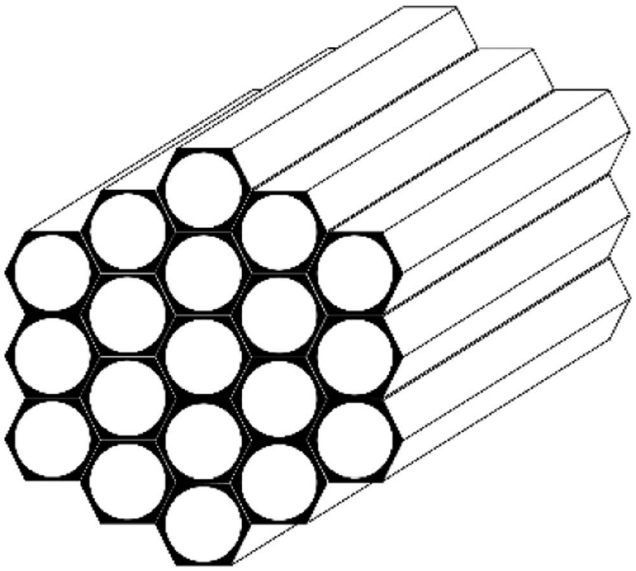

Fig. 1 The pore structure of MCM-41.

the above literatures, only the changes in physical properties of MCM-41 was emphasized in membrane preparation processes, and the compatibility between polymer and MCM-41 by chemical bridging was ignored. In addition, to our best knowledge, only a few works about MCM-41 MMMs focused on the separation of *n*-butanol from the *n*-butanol/water mixture.[26,27] In our previous work, surface modified silicalite-1 was synthesized as a macro-crosslinker for MMMs preparation, which not only provided permselective channels for *n*-butanol molecules, but also reacted with the hydroxyl groups of PDMS during the membrane preparation process. Nevertheless, because of the relatively low diameter of these channels, the flux improvement was not obvious when used the modified silicalite-1 as the crosslinker.[28,29]

In the current work, aiming to incorporate MCM-41 into PDMS membrane to improve the flux, different types of silane coupling agents were applied to modify MCM-41. The modified MCM-41 could eliminate the inhibiting effect of the active silanols on the surface of MCM-41. Therefore, the curing process was improved significantly. Moreover, the silane coupling agents were used to form the covalent bonds between MCM-41 and PDMS. The compatibility was improved and the interfacial gap was eliminated between particles and polymers in the process of MMMs preparation.[30–32] The morphologies and chemical structures of the MCM-41 and MCM-41/PDMS MMMs was analyzed by Fourier transform infrared spectroscopy (FTIR), transmission electron microscope (TEM), scanning electron microscope (SEM), Brunauer–Emmett–Teller (BET), contact angle measurement and rheology measurement. The separation performances of the MCM-41/PDMS MMMs modified by different types of silane coupling agents were compared using 1.5 wt% *n*-butanol/H_2O binary mixture in feed. The improvement of the curing process of MCM-41/PDMS (hydroxyl-terminated PDMS) membrane by incorporating multi-silyl-functional MCM-41 was investigated for the first time. The optimal MMMs could not only exhibit significant improvements of flux, but also facilitate the curing process in membrane preparation, which showed a promising prospect for effective *n*-butanol separation.

Experimental section

Materials

MCM-41 (Xianfeng Nano Technology, Nanjing, China) was used as the molecular sieve. And tetraethyl orthosilicate (TEOS, ≥99.5%) (Xilong Chemicals, Guangdong, China) and dibutyltin dilaurate (DBTDL, ≥99.0%) (Fuchen Chemicals, Tianjing, China) were used as crosslinking agent and catalyst, respectively. Hydroxyl terminated PDMS was obtained from Shandong Dayi Chemical Co., Ltd. *N*-Propyltrimethoxysilane (PTMS, 97%), *n*-octyltrimethoxysilane (OTMS, 97%), and *n*-dodecyltrimethoxysilane (DTMS, 97%) were purchased from Sinopharm Chemical Reagent Co., Ltd. and *n*-hexadecyltrimethoxysilane (HDTMS, 98%) were purchased from Xiya Chemical Industry Co., Ltd.

Surface modification of MCM-41 particles

10 g of MCM-41 and the excess silane coupling agents were dissolved in 150 g of *n*-heptane. The mixture was sealed and kept for 48 h at 80 °C under magnetic stirring. The particles were then washed by *n*-heptane (centrifugation and decanting of supernatant). After dried out in vacuum at 100 °C, the multi-silyl-functional MCM-41 particles were collected and were used for MMMs preparation.

Membrane preparation

The PDMS polymer, TEOS and 20 wt% of unmodified or modified MCM-41 particles were dissolved in *n*-hexane, followed by stirred at room temperature at 1000 rpm for 2 h. The DBTDL was then added into the mixture. After 10 min of stirring, the resulted mixture was cast on the laboratory-made PVDF membrane using an automatic coating machine (Elcometer 4340, UK) and subsequently kept at 80 °C for 24 h.

Characterization of MCM-41 particles and membranes

The morphology of MCM-41 particles was performed by employing a transmission electron microscope (TEM, JEM-2100F, Japan). The morphology of the surface and cross-sectional morphology of membranes were obtained by employing a scanning electron microscope (SEM, SU8020, Hitachi High-Technologies Corporation, Japan). The water contact angles on the surface of MMMs were measured by a contact angle measurement (JC2000D, Shanghai Zhongchen Corporation, China). The rheology of MMMs curing was carried out on a rheometer (AR2000ex, TA Instruments, USA). To test the chemical groups of MCM-41 particles, a Fourier transform infrared spectroscopy (FTIR, Varian-3100, Varian Inc., USA) was employed. Autosorb-iQ specific surface area analyzer (Quantachrome, USA) was employed to study the pore size and specific surface area of MCM-41 particles before and after modification. The methods were as follow: the samples were degassed at 250 °C and 10^{-3} Torr for 3 h and the adsorption and desorption

isotherms were measured at 77.4 K. The pore size distribution was calculated by BJH and DFT methods.

Static adsorption experiment

About 1 g MCM-41 particles were added to a pre-weighed weighing bottle. The weighing bottle with the samples was placed in a vacuum oven and degassed at 200 °C for 6 h. After degassed, the weighing bottle was quickly and accurately weighed. The bottle was then placed in a desiccator containing a *n*-butanol aqueous solution. And the desiccator was sealed in a constant temperature oven at 35 °C for 24 h. The weight is accurately weighed and the static adsorption capacity of molecular sieve samples on *n*-butanol (x) was calculated by the following equation:

$$x(\%) = \frac{m_3 - m_2}{m_2 - m_1} \times 100 \quad (1)$$

where m_1 and m_2 are the weight of the weighing bottle and the total weight of sample and weighing bottle after degassed (g), respectively. m_3 represents the total weight of sample and weighing bottle after adsorption (g). Samples were repeated in duplicates. The static saturation of H_2O adsorption capacities of multi-silyl-functional MCM-41 particles were measured in similar ways.

Pervaporation experiments

The membranes were tested in a pervaporation system that was described in detail in previous work.[33] The effective area of the membrane is 30.19 cm^2. 6 L of 1.5 wt% *n*-butanol/water model solution was kept in a stainless steel tank. The pressure on the permeate side of the pervaporation membrane was kept below 150 Pa. The feed temperature was maintained at 55 °C. The permeate was collected by a liquid nitrogen trap. Gas chromatograph (GC-14C, Shimadzu Corporation, Japan) was used to analyze the *n*-butanol concentrations. And the experiments were carried out in triplicates.

Total flux (J), *n*-butanol flux ($J_{butanol}$), water flux (J_{water}), separation factor (β), *n*-butanol permeance ($P_{butanol}/\ell$), water permeance (P_{water}/ℓ), selectivity (α), and permeate concentration ($y_{butanol}$) were used to evaluate the separation performance of membranes, which were calculated by following equations:[34]

$$J = \frac{W}{A \times \Delta t} \quad (2)$$

$$J_{butanol} = J \times y_{butanol} \quad (3)$$

$$J_{water} = J \times (1 - y_{butanol}) \quad (4)$$

$$\beta = \frac{y_{butanol}/(1 - y_{butanol})}{x_{butanol}/(1 - x_{butanol})} \quad (5)$$

$$\frac{P_{butanol}}{\ell} = j_{butanol} \times \frac{1}{\mathcal{P}^{f}_{butanol} - \mathcal{P}^{p}_{butanol}} = J_{BuOH} \times \frac{V_m}{M_{butanol}\left(\mathcal{P}^{f}_{butanol} - \mathcal{P}^{p}_{butanol}\right)} \quad (6)$$

$$\frac{P_{water}}{\ell} = j_{water} \times \frac{1}{\mathcal{P}^{f}_{water} - \mathcal{P}^{p}_{water}} = J_{water} \times \frac{V_m}{M_{water}(\mathcal{P}^{f}_{water} - \mathcal{P}^{p}_{water})} \quad (7)$$

$$\alpha = \frac{P_{butanol}}{P_{water}} \quad (8)$$

where W is the weight of the permeate (g) collected over time Δt (h) of the effective area A (m^2); $j_{butanol}$ and j_{water} represent the volume fluxes of *n*-butanol and water (cm^3(STP) cm^{-2} s^{-1}), respectively; ℓ and V_m refer to the membrane thickness (cm) and the molar volume of gas (22.4 L mol^{-1}, STP), respectively; the molecular weights of *n*-butanol and water are represented by $M_{butanol}$ and M_{water}, respectively; $\mathcal{P}^{f}_{butanol}$, $\mathcal{P}^{p}_{butanol}$, $\mathcal{P}^{f}_{water}$ and $\mathcal{P}^{p}_{water}$ are the vapor partial pressures of *n*-butanol and water in the feed and the permeate, respectively. The vapor partial pressures of *n*-butanol and water in the feed were obtained from Aspen Plus V8.0 applied by the NRTL model. The overall performance of the membrane was indicated by a pervaporation separation index (PSI) as following equation:

$$PSI = J \times (\beta - 1) \quad (9)$$

Results and discussion

Characterization of multi-silyl-functional MCM-41 particles

The morphology and microstructure of MCM-41 particles were observed by TEM (Fig. 2a). The MCM-41 particles were ordered one-dimensional linear channels like "honeycomb". And the morphology was consistent with Fig. 1. A narrow pore size distribution of MCM-41 particles was observed in Fig. 2b and the average pore size was 2.815 nm. Therefore, the pore sizes of MCM-41 particles were large enough for *n*-butanol diffusion. Furthermore, the MCM-41 had a high BET surface area and pore volume of 1657 m^2 g^{-1} and 1.425 cm^3 g^{-1}, respectively.

PTMS-MCM-41, OTMS-MCM-41, DTMS-MCM-41 and HDTMS-MCM-41 represent the MCM-41 particles modified by PTMS, OTMS, DTMS and HDTMS, respectively. Scheme 1 shows the surface modification mechanism of MCM-41 by silane coupling agents. As illustrated, the MCM-41 surface was functioned with alkyl and methoxyl groups. As a result, the hydrophobicity of MCM-41 surface was significantly improved by the effect of the functional groups.

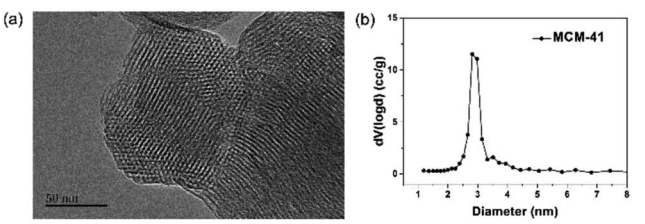

Fig. 2 (a) The TEM image of MCM-41 and (b) its BJH pore size distribution.

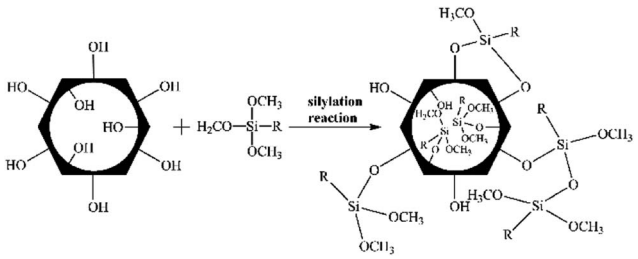

Scheme 1 The surface modification mechanism for MCM-41 with silane coupling agents. R represents alkyl group.

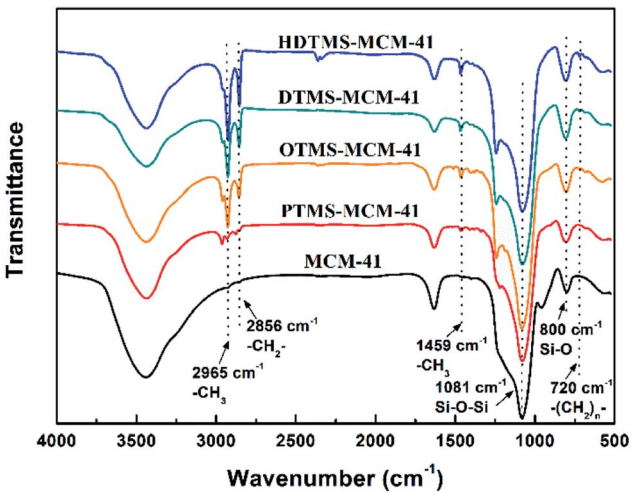

Fig. 3 The FTIR spectra of the MCM-41 before and after silylated modification.

FTIR were used to analyze the chemical structure of MCM-41 after modification. As shown in Fig. 3, the absorption peaks at 2965 cm^{-1} and 2856 cm^{-1} were observed in all the spectra of the multi-silyl-functional MCM-41, which were attributed to the stretching vibrations of $-CH_3$ and $-CH_2-$ groups, respectively.[35,36] Compared to unmodified MCM-41, the peak located at 1459 cm^{-1} was due to the bending vibration of $-CH_3$ group. And the peak located at 720 cm^{-1} was related to the bending vibration of the $-(CH_2)_n-$ groups. The increasing intensity of these peaks from PTMS-MCM-41 to HDTMS-MCM-41 was attributed to the increase of the chain length of alkyl groups. These confirmed the successful silylation of MCM-41. Additionally, the absorption peaks of Si–OH groups located at 3440 cm^{-1} was weaker after surface modification. Moreover, the absorption peaks at 1081 cm^{-1} and 800 cm^{-1} were attributed to the stretching vibrations of Si–O–Si and Si–O groups, respectively.

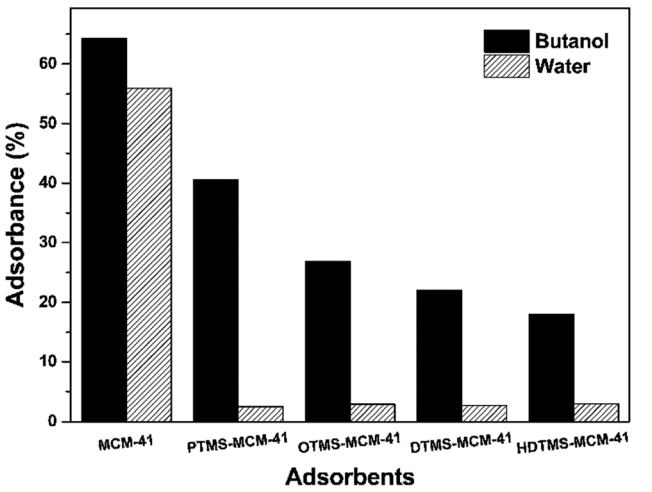

Fig. 4 The absorption capacity of the MCM-41 before and after silylated modification.

The pore size, pore volume and specific surface area of the multi-silyl-functional MCM-41 particles were shown in Table 1. It indicated that the pore sizes and porosities of the MCM-41 molecular sieves were gradually decreased with the increase of the alkyl chain length of the silane coupling agents. The three-dimensional size of PTMS, OTMS, DTMS and HDTMS were 5.774 × 5.607 × 5.531 Å, 7.050 × 7.799 × 8.416 Å, 10.254 × 7.113 × 8.322 Å and 13.875 × 15.916 × 12.232 Å, respectively (calculated by Materials Studio 7.0). The pore diameter of MCM-41 was larger than the silane coupling agent molecules. Therefore, silane coupling agent molecules successfully entered into the inner channels of MCM-41.

Hence, both the outer surface and inner surface of MCM-41 could be modified by the silane coupling agents.[37] With the increase of the alkyl chain length, the pore space of the multi-silyl-functional MCM-41 was decreased, which further resulted in the drop of its pore size and pore volume. At the same time, the specific surface area of the multi-silyl-functional MCM-41 was reduced due to the reduction of the pore volume. And the pore structures of the multi-silyl-functional MCM-41 could be adjusted by bridging silane coupling agents with different chain lengths.

The absorption capacity of the MCM-41 before and after modification was investigated and the results are shown in Fig. 4. The unmodified MCM-41 showed a high adsorption capacity volume and poor *n*-butanol selectivity. Because the presence of abundant Si–OH in the MCM-41 channels before modification, the pores were quite hydrophilic. Therefore, water

Table 1 The pore structure properties of the MCM-41 before and after modification

Sample	S_{BET} (m^2 g^{-1})	V_p (cm^3 g^{-1})	BJH D_{pore} (nm)	DFT D_{pore} (nm)
MCM-41	1657	1.425	2.815	3.030
PTMS-MCM-41	1303	0.843	1.873	2.313
OTMS-MCM-41	1004	0.607	1.356	1.847
DTMS-MCM-41	640	0.445	1.360	1.475
HDTMS-MCM-41	56	0.181	—	—

Table 2 The effect of the addition of MCM-41 on the membrane curing process

Fillers	The composition of the casting solution (PDMS : TEOS : DBTDL)	The state of the casting solution (curing time)
None	5.5 : 0.3 : 0.015	Cured (2500 s)
20% MCM-41	5.5 : 0.3 : 0.015	Uncured
20% MCM-41	5.5 : 0.3 : 0.045	Uncured
20% MCM-41	5.5 : 0.9 : 0.015	Cured (40 h)
20% MCM-41	5.5 : 0.9 : 0.045	Cured (29 h)
20% modified MCM-41[a]	5.5 : 0.3 : 0.015	Cured (~4000 s)

[a] Modified MCM-41: the MCM-41 modified by PTMS, OTMS, DTMS and HDTMS, respectively.

molecules were easily absorbed into their pores and the pores resistances to water molecules were weak. However, the adsorption capacity of water in the modified MCM-41 was quite different from that in unmodified MCM-41. The water adsorption was decreased from 55% to 2–3%. The alkyl chain, which was loaded into the MCM-41 pores, enhanced the hydrophobic interaction so that it could effectively prevent water from entering into the channels.

Saturated adsorption capacity of *n*-butanol was gradually decreased with the increase of the alkyl chain length in the silane coupling agents. It was caused by the decrease of the pore volume with the alkyl chain length. However, the alkyl chain length showed little influence on water adsorption.

Preparation of MMMs using surface multi-silyl-functional MCM-41 as a crosslinker

MCM-41 particles were filled into PDMS to prepare the MMMs. The particles loading content $[W_{\text{MCM-41}}/(W_{\text{MCM-41}} + W_{\text{PDMS}})]$ was 20 wt%. It is worthy to note here that the curing process of the MCM-41/PDMS membrane was quite different from that of the pure PDMS membrane.[38,39] Interestingly, the casting solution was not cured after a long time (up to 3 days) when unmodified MCM-41 was filled into PDMS.

In order to explore the curing process of PDMS membrane incorporating MCM-41, the contrastive experiments were carried out by changing the composition of the casting solution. The results are shown in Table 2. Schematic representation of crosslinking reaction of PDMS membrane is shown in Scheme 2a. When MCM-41 was not filled, the casting solution was completely cured after only 40 minutes. On the contrary, the casting solution was not cured over 3 days after filling 20 wt% unmodified MCM-41. Subsequently, by increasing the concentration of catalyst DBTDL, the increase rate of the casting solution's viscosity was increased, though the PDMS was still not cured. This implied the addition of MCM-41 didn't affect the activity of the catalyst. The casting solution was cured after 40 h reactions when increasing the concentration of TEOS. The curing time was also shortened by simultaneously increasing the concentrations of TEOS and DBTDL. Therefore, the MCM-41 only hindered the cross-linking reaction between TEOS and PDMS. The possible reason for this phenomenon might be the three different silicon hydroxyl groups (isolated, geminal and

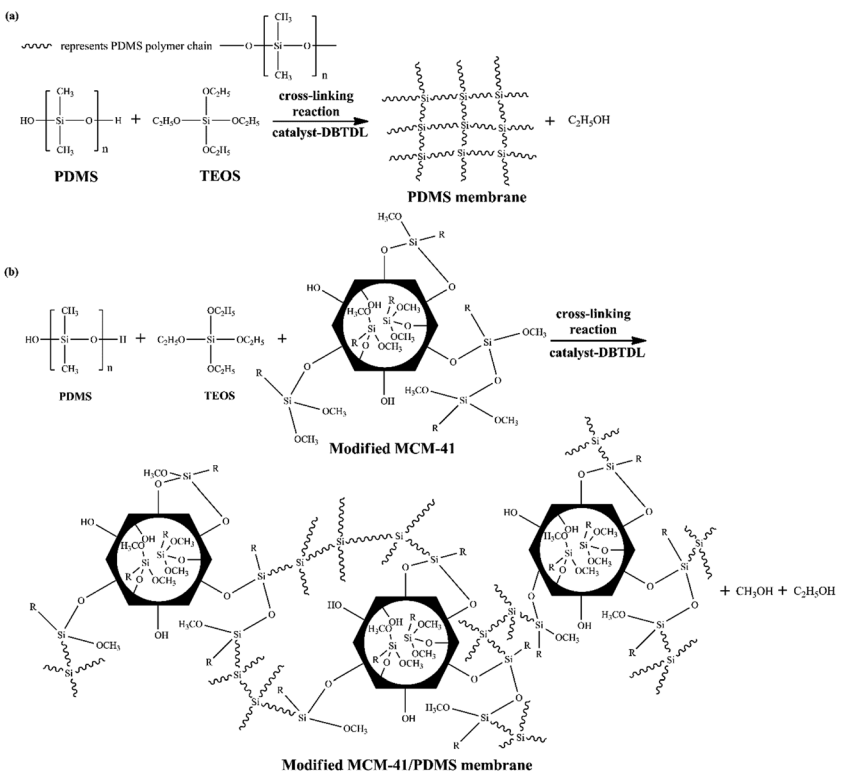

Scheme 2 Crosslinking reaction of (a) PDMS membrane and (b) modified MCM-41/PDMS membrane. R represents an alkyl chain.

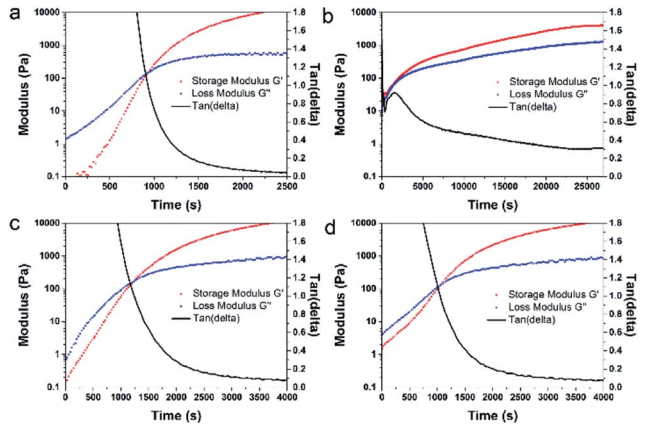

Fig. 5 Rheology of (a) the PDMS membrane, (b) 20 wt% MCM-41/PDMS membrane, (c) 20 wt% DTMS-MCM-41/PDMS membrane and (d) 20 wt% HDTMS-MCM-41/PDMS membrane. The storage modulus G' and the loss modulus G'' refer to the elastic and viscous portion, respectively. Polymer solution is a solid state when the storage modulus G' is much higher than the loss modulus G''. On the contrary, when the storage modulus G' is much lower than the loss modulus G'', polymer solution is a liquid state.

hydrogen-bonded silanols) on the inner and outer surfaces of MCM-41 molecular sieves.[40] The isolated and geminal silanols can easily react with $-OC_2H_5$ of TEOS. As a result, the active silanols on the surface of MCM-41 competitively inhibited the polymerization of PDMS and TEOS.

To further explore the curing process, the rheology of casting solution during the curing process was evaluated. As shown in Fig. 5a, after the addition of the catalyst, the G' and G'' of the casting solution without adding MCM-41 increased with the increase of reaction time. When G' and G'' met at the crossover point (at about 900 s), the reaction mixture changed from liquid state to solid state.[41] After 2500 s of reaction, the loss tangent ($\tan(\text{delta}) = G''/G'$) of the casting solution reached 0.043, indicating that G' of mixture was much larger than G''. On this condition, the casting solution was under solid state. As illustrated in Fig. 5b, the casting solution with additional 20 wt% unmodified MCM-41 reached the transition state much faster. However, the loss tangent of the casting solution only was 0.3. It was maintained at a semi-solid state after a long time (>25 000 s). Therefore, the addition of unmodified MCM-41 hindered the cross-linking reaction between PDMS polymer chains and TEOS.

For the purpose of eliminating the inhibiting effect of the active silanols and further improving the curing process and compatibility between MCM-41 and PDMS, the multi-silyl-functional MCM-41 were added into the casting solution. As shown in Table 2, the casting solution cured. As illustrated in Scheme 2b, after modification, the active silanol groups on the MCM-41 surface were replaced by the functional groups of alkyl and methoxyl. These groups could significantly reduce the inhibiting effect of active silanols on the surface of MCM-41. Therefore, the curing time (~4000 s) was shortened observably compared to the case of incorporating unmodified MCM-41 into PDMS (40 h, 29 h). Moreover, the curing time of modified-MCM-41/PDMS solution was a little longer than that of the pure PDMS solution. The possible reason might be the residual silanol groups on the surfaces of MCM-41 particles, which did not react with silane coupling agents effectively.

In the curing process of PDMS membrane or MCM-41/PDMS membrane, TEOS served as a crosslinkers to react with PDMS chains (Scheme 2a). And the unmodified MCM-41 were physically embedded into polymer phase. As indicated in our previous work,[28] the compatibility between unmodified MCM-41 and PDMS was poor. In contrast, in the curing process of modified MCM-41/PDMS membrane, the multi-silyl-functional MCM-41 also served as a crosslinker to react with PDMS. The grafted silane groups on the surface of multi-silyl-functional MCM-41 reacted with the terminal hydroxyl groups of PDMS chains. On this way, the multi-silyl-functional MCM-41, TEOS, and PDMS were linked with each other to form a complex network. This was consistent with the rheology results shown in Fig. 5c and d. In the curing process of modified MCM-41/PDMS membrane solutions (DTMS-MCM-41/PDMS and HDTMS-MCM-41/PDMS), G' increased rapidly with the increase of crosslinking time. The loss tangent of two casting solutions reduced to 0.1 or less (at about 4000 s). As expect, the solutions were soon completely converted into the solid state, demonstrating that the silylated modification could significantly reduce the active Si–OH on the surface of MCM-41 and further effectively eliminate the competitive inhibition during PDMS cross-linking. Besides, the interfacial gap between PDMS and modified-MCM-41 was also eliminated through the Si–O–Si covalent bonds.

Pervaporation performance

The SEM images and water contact angles of PDMS membrane and modified MCM-41/PDMS membranes are shown in Fig. 6. It indicated that the multi-silyl-functional MCM-41 particles easily formed irregular agglomeration in the PDMS polymer matrix. However, with the increase of the grafted alkyl chain length, the hydrophobic interaction of the multi-silyl-functional MCM-41 was enhanced, leading to an enhancement of the dispersity in PDMS. In addition, the water contact angles in Fig. 6 indicated that the surface hydrophobicity of modified MCM-41/PDMS membranes was much higher than that of pure PDMS

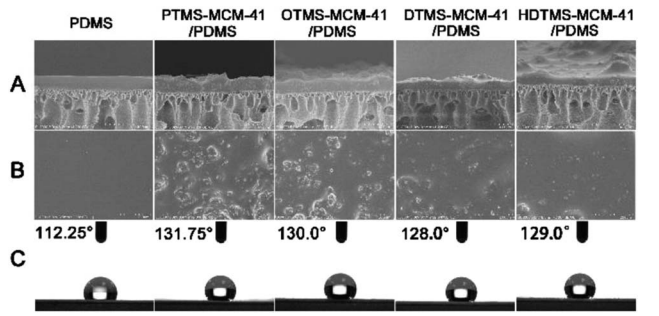

Fig. 6 Cross-section (A), surface (B) SEM images and water contact angles (C) of PDMS membrane and 20 wt% modified MCM-41/PDMS membranes.

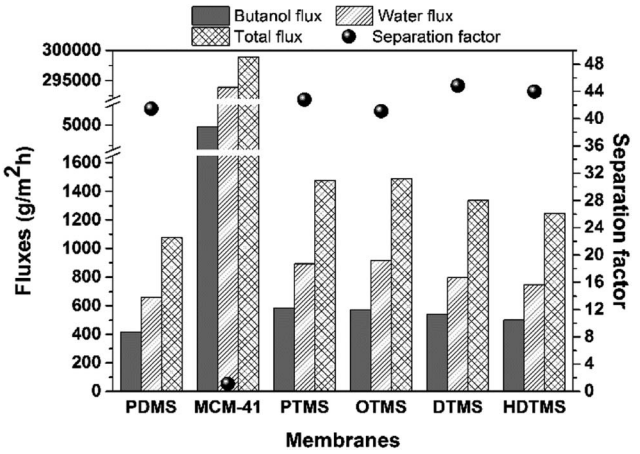

Fig. 7 The flux and separation factor of the modified MCM-41/PDMS membranes for separating 1.5 wt% *n*-butanol aqueous solution at 55 °C.

membrane. These results demonstrated that bonding the multi-silyl-functional MCM-41 with PDMS could significantly enhance the hydrophobic interaction, although the length of the alkyl chain of the silane coupling agents showed little influences.

The effects of modification of MCM-41 on the *n*-butanol separation performance were also investigated. As shown in Fig. 7, the total flux, *n*-butanol flux and water flux of PTMS-MCM-41/PDMS, OTMS-MCM-41/PDMS, DTMS-MCM-41/PDMS and HDTMS-MCM-41/PDMS membranes were always higher than that of pure PDMS membrane, indicating that the multi-silyl-functional MCM-41 molecular sieves provided suitable mass transfer "channels" for *n*-butanol separation. Among them, PTMS-MCM-41/PDMS membrane showed the highest total flux of 1476 g m^{-2} h^{-1} and *n*-butanol flux of 582 g m^{-2} h^{-1}. On these condition, the total flux increased by nearly 40% compared with pure PDMS membrane (1075 g m^{-2} h^{-1}). In fact, PTMS-MCM-41 possessed the largest pore volume and pore diameter compared to other modified MCM-41 particles, which resulted in the most effective molecules transfer.

MCM-41/PDMS membrane showed the total flux of 298 883 g m^{-2} h^{-1}, *n*-butanol flux of 4980 g m^{-2} h^{-1} and water flux of 293 902 g m^{-2} h^{-1}, respectively, which were much higher than that of pure PDMS membrane and modified MCM-41/PDMS membranes. However, the separation factor of MCM-41/PDMS membrane was only 1.11. In fact, the curing time of 20 wt% MCM-41/PDMS solution (29 h, as shown in Table 2) from liquid state to solid state was too long in membrane preparation process. PDMS could not cure at the appropriate time. As shown in Fig. 8, compared with PDMS and modified MCM-41/PDMS membranes, there was no dense and continuous membrane structure. On the contrary, there were obvious interfacial defects and gaps. The uncured PDMS polymer may gradually permeate into PVDF finger-like pores layer with the increase of the curing time, while MCM-41 particles were deposited on the top of MMM. Some MCM-41 particles even could not stick to PDMS. Therefore, the total flux of MCM-41/PDMS membrane was much higher than that of pure PDMS and modified MCM-41/PDMS membranes, and the separation factor was very low.

It was found that bonding multi-silyl-functional MCM-41 with PDMS could not effectively improve the separation factor of *n*-butanol. It might be attributed to the similar selective transport "channels" to PDMS matrix, only based on hydrophobic interaction.[23] The permeance and selectivity of modified MCM-41/PDMS membranes were shown in Fig. 9. The *n*-butanol permeance increased significantly compared to pure PDMS membrane due to the addition of multi-silyl-functional MCM-41. With the decrease of the pore size of modified MCM-41 molecular sieves, the *n*-butanol and water permeance of the modified-MCM-41/PDMS membranes were decreased gradually. In contrast, the selectivity of *n*-butanol was also slightly improved. Moreover, the high permeance and low selectivity of MCM-41/PDMS membrane were consistent with its high flux and low separation factor.

Table 3 summarized the current advances of the pervaporation membranes for effective *n*-butanol separation from model solutions. As shown in the Table 3, the 20 wt% PTMS-MCM-41/PDMS membrane exhibited attractive flux and *n*-butanol separation factor. As expected, MCM-41 was modified by different types of silane coupling agents to enhance surface hydrophobicity so that the dispersity was effectively improved in PDMS membrane. Importantly, multi-silyl-functional MCM-41 as a crosslinker could eliminate the interfacial gap and improve the compatibility between particles and polymers. As a result, the highest PSI of 61 992 was also obtained in the current work,

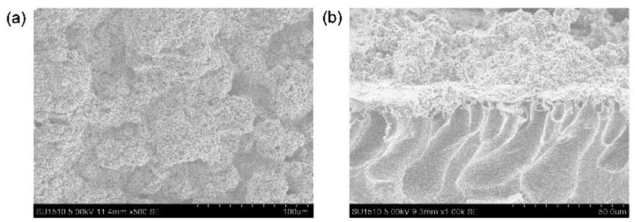

Fig. 8 Surface (a) and cross-section (b) SEM images of 20 wt% MCM-41/PDMS membranes (PDMS : TEOS : DBTDL = 5.5 : 0.9 : 0.045).

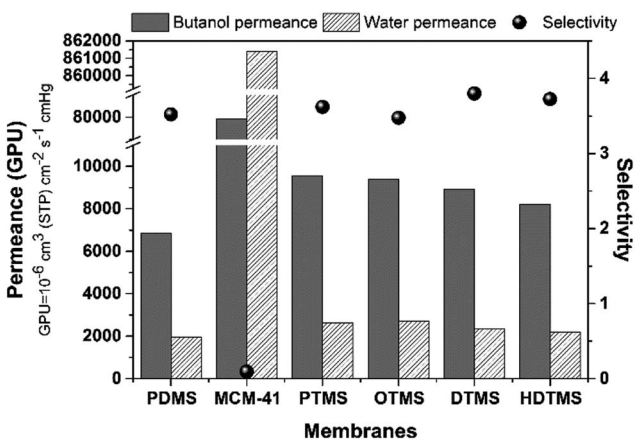

Fig. 9 The permeance and selectivity of the modified MCM-41/PDMS membranes for separating 1.5 wt% *n*-butanol aqueous solution at 55 °C.

Table 3 Current advances of the pervaporation membranes for effective *n*-butanol separation from model solutions

Membranes	Particle loading (wt%)	Feed temp. (°C)	Feed *n*-butanol content (wt%)	Total flux (g m^{-2} h^{-1})	Separation factor	PSI	Ref.
ZIF-71/PEBA	20	40	1	~86	~20	1634	16
Silicalite-1/PDMS	60	50	1	191	113	21 411	42
ZSM-5/PDMS	30	35	6	104	38	3848	43
Silicalite-1/PDMS	65	80	1.9	65	47	2990	44
MCM-41/PEBA	2	35	2.5	~500	~25	12 048	26
PDMS/PAN		42	1	1390	22	33 341	45
PDMS		55	1.5	1075	41	43 000	This study
PTMS-MCM-41/PDMS	20	55	1.5	1476	43	61 992	This study

which was ~1.5 times higher than that of pure PDMS (43 000, in the control group). In consideration of the high flux and the overall techno-economic feasibility, the 20 wt% PTMS-MCM-41/PDMS membrane showed promising in practical applications.

Conclusion

Multi-silyl-functional MCM-41 as a molecular sieve showed superiority for MMMs preparation. The curing process for membrane preparation was significantly improved. After silylated modification, the modified MCM-41 showed better compatibility in the casting solution, providing high membrane flux and *n*-butanol separation factor. The novel modified MCM-41/PDMS MMMs showed promising in effective *n*-butanol separation from diluted aqueous and fermentation broth.

Conflicts of interest

There are no conflicts to declare.

Acknowledgements

This work was supported in part by the National Nature Science Foundation of China (Grant No. 21476015, 21676014, and 21706008), Beijing Natural Science Foundation (2172041) and China Postdoctoral Science Foundation (2017M610037).

Notes and references

1 L. Y. Jiang, Y. Wang, T.-S. Chung, X. Y. Qiao and J.-Y. Lai, *Prog. Polym. Sci.*, 2009, **34**, 1135–1160.
2 D. T. Jones and D. R. Woods, *Microbiol. Rev.*, 1986, **50**, 484.
3 N. Qureshi and T. C. Ezeji, *Biofuels, Bioprod. Biorefin.*, 2008, **2**, 319–330.
4 L. M. Vane, *J. Chem. Technol. Biotechnol.*, 2005, **80**, 603–629.
5 D. Cai, H. Chen, C. Chen, S. Hu, Y. Wang, Z. Chang, Q. Miao, P. Qin, Z. Wang, J. Wang and T. Tan, *Chem. Eng. J.*, 2016, **287**, 1–10.
6 D. Cai, Z. Dong, J. Han, H. Yu, Y. Wang, P. Qin, Z. Wang and T. Tan, *Green Chem.*, 2016, **18**, 1377–1386.
7 D. Cai, P. Li, C. Chen, Y. Wang, S. Hu, C. Cui, P. Qin and T. Tan, *Bioresour. Technol.*, 2016, **220**, 68–75.
8 L. M. Robeson, *J. Membr. Sci.*, 2008, **320**, 390–400.
9 Y. Li, H. Zhou, G. Zhu, J. Liu and W. Yang, *J. Membr. Sci.*, 2007, **297**, 10–15.
10 K. Li, *Ceramic Membranes for Separation and Reaction*, John Wiley, 2010.
11 S.-Y. Li, R. Srivastava and R. S. Parnas, *J. Membr. Sci.*, 2010, **363**, 287–294.
12 B. Zornoza, P. Gorgojo, C. Casado, C. Téllez and J. Coronas, *Desalin. Water Treat.*, 2011, **27**, 42–47.
13 B. Zornoza, O. Esekhile, W. J. Koros, C. Téllez and J. Coronas, *Sep. Purif. Technol.*, 2011, **77**, 137–145.
14 B. Zornoza, C. Tellez, J. Coronas, J. Gascon and F. Kapteijn, *Microporous Mesoporous Mater.*, 2013, **166**, 67–78.
15 E. A. Fouad and X. Feng, *J. Membr. Sci.*, 2009, **339**, 120–125.
16 S. Liu, G. Liu, X. Zhao and W. Jin, *J. Membr. Sci.*, 2013, **446**, 181–188.
17 J. A. Thompson, K. W. Chapman, W. J. Koros, C. W. Jones and S. Nair, *Microporous Mesoporous Mater.*, 2012, **158**, 292–299.
18 H. Fan, N. Wang, S. Ji, H. Yan and G. Zhang, *J. Mater. Chem. A*, 2014, **2**, 20947–20957.
19 H. Sun, L. Lu, X. Chen and Z. Jiang, *Sep. Purif. Technol.*, 2008, **58**, 429–436.
20 M. J. C. Ordoñez, K. J. Balkus, J. P. Ferraris and I. H. Musselman, *J. Membr. Sci.*, 2010, **361**, 28–37.
21 B. Van der Bruggen and P. Luis, *Curr. Opin. Chem. Eng.*, 2014, **4**, 47–53.
22 Q. Cai, Z.-S. Luo, W.-Q. Pang, Y.-W. Fan, X.-H. Chen and F.-Z. Cui, *Chem. Mater.*, 2001, **13**, 258–263.
23 L. Wang, X. Han, J. Li, L. Qin and D. Zheng, *Powder Technol.*, 2012, **231**, 63–69.
24 A. Jomekian, S. A. A. Mansoori and N. Monirimanesh, *Desalination*, 2011, **276**, 239–245.
25 S. D. Bhat, B. V. K. Naidu, G. Shanbhag, S. B. Halligudi, M. Sairam and T. M. Aminabhavi, *Sep. Purif. Technol.*, 2006, **49**, 56–63.
26 H. Tan, Y. Wu, Y. Zhou, Z. Liu and T. Li, *J. Membr. Sci.*, 2014, **453**, 302–311.
27 N. Wang, G. Shi, J. Gao, J. Li, L. Wang, H. Guo, G. Zhang and S. Ji, *Sep. Purif. Technol.*, 2015, **153**, 146–155.
28 S. Hu, W. Ren, D. Cai, T. C. Hughes, P. Qin and T. Tan, *J. Membr. Sci.*, 2017, **533**, 270–278.
29 D. Cai, S. Hu, C. Chen, Y. Wang, C. Zhang, Q. Miao, P. Qin and T. Tan, *Bioresour. Technol.*, 2016, **220**, 124–131.

30 O. G. Nik, X. Y. Chen and S. Kaliaguine, *J. Membr. Sci.*, 2011, **379**, 468–478.
31 J. Yang, C.-R. Han, J.-F. Duan, F. Xu and R.-C. Sun, *J. Phys. Chem. C*, 2013, **117**, 8223–8230.
32 A. L. Khan, C. Klaysom, A. Gahlaut and I. F. J. Vankelecom, *J. Membr. Sci.*, 2013, **436**, 145–153.
33 S. Hu, Y. Guan, D. Cai, S. Li, P. Qin, M. N. Karim and T. Tan, *Sci. Rep.*, 2015, **5**, 9428.
34 R. W. Baker, J. G. Wijmans and Y. Huang, *J. Membr. Sci.*, 2010, **348**, 346–352.
35 S. A. Kulkarni, S. B. Ogale and K. P. Vijayamohanan, *J. Colloid Interface Sci.*, 2008, **318**, 372–379.
36 J. Chen, Q. Li, R. Xu and F. Xiao, *Angew. Chem., Int. Ed.*, 1995, **34**, 2694–2696.
37 X. Zhao and G. Lu, *J. Phys. Chem. B*, 1998, **102**, 1556–1561.
38 F. Qin, S. Li, P. Qin, M. N. Karim and T. Tan, *Green Chem.*, 2014, **16**, 1262–1273.
39 S. Li, F. Qin, P. Qin, M. N. Karim and T. Tan, *Green Chem.*, 2013, **15**, 2180.
40 X. S. Zhao, G. Q. Lu, A. K. Whittaker, a. G. J. Millar and H. Y. Zhu, *J. Phys. Chem. B*, 1997, **101**, 6525–6531.
41 F. Chambon and H. H. Winter, *Polym. Bull.*, 1985, **13**, 499–503.
42 J. Huang and M. Meagher, *J. Membr. Sci.*, 2001, **192**, 231–242.
43 I. F. Vankelecom, D. Depre, S. De Beukelaer and J. B. Uytterhoeven, *J. Phys. Chem.*, 1995, **99**, 13193–13197.
44 C. Xue, F. Liu, M. Xu, I. C. Tang, J. Zhao, F. Bai and S. T. Yang, *Bioresour. Technol.*, 2016, **219**, 158–168.
45 J. Niemistö, W. Kujawski and R. L. Keiski, *J. Membr. Sci.*, 2013, **434**, 55–64.